Jianjian Wei., Lei Wang., Tao Jin., Yuguo Li., Nan Zhang. (2022).
Effects of occupant behavior and ventilation on exposure to respiratory droplets in the indoor environment. *Building and Environment*.

Effects of occupant behavior and ventilation on exposure to respiratory droplets in the indoor environment

Jianjian Wei
Lei Wang
Tao Jin
Yuguo Li
Nan Zhang

Institute of Refrigeration and Cryogenics, Key Laboratory of Refrigeration and Cryogenic Technology of Zhejiang Province, Zhejiang University, Hangzhou, China
Jiaxing Research Institute, Zhejiang University, Jiaxing, China
Department of Mechanical Engineering, The University of Hong Kong, Hong Kong, China
Beijing Key Laboratory of Green Built Environment and Energy Efficient Technology, Beijing University of Technology, Beijing, China

Corresponding author:Beijing University of Technology, Beijing, China.
E-mail address: zhangn@bjut.edu.cn (N. Zhang).

Submitted to *Building and Environment* 14 October 2022
Accepted 31 December 2022

Author biographies

Jianjian Wei, PhD, is Associate Professor in the Institute of Refrigeration and Cryogenics and Key Laboratory of Refrigeration and Cryogenic Technology of Zhejiang Province, Zhejiang University, Hangzhou, China. His research interests are in aerosol dynamics and indoor airborne transmission of pathogens. His current research topics include short-range airborne infection risks in close-contact scenarios, fecal aerosol dispersion in high-rise buildings, and bioaerosol stability under varying environmental conditions.

Lei Wang, is a researcher in Institute of Refrigeration and Cryogenics, Key Laboratory of Refrigeration and Cryogenic Technology of Zhejiang Province, Zhejiang University.

Tao Jin, is a researcher in Institute of Refrigeration and Cryogenics, Key Laboratory of Refrigeration and Cryogenic Technology of Zhejiang Province, Zhejiang University.

Yuguo Li, PhD, is Chair Professor of Building Environment, Honorary Professor of School of Public Health, Associate Dean (Research) of Engineering. His research interests are in building environment engineering. His current research topics include city climate/environment, environment studies of infection and indoor environment.

Nan Zhang, PhD, is Professor in the College of Architecture and Civil Engineering at Beijing University of Technology. His research interests are in building environment and human behaviour. His current research topics include healthy buildings and intelligent building systems.

Effects of occupant behavior and ventilation on exposure to respiratory droplets in the indoor environment

Abstract

To quantify the risk of the transmission of respiratory infections in indoor environments, we systematically assessed exposure to talking- and breathing-generated respiratory droplets in a generic indoor environment using computational fluid dynamic (CFD) simulations. The flow field in the indoor environment was obtained with SST k-ω model and Lagrangian method was used to predict droplet trajectories, where droplet evaporation was considered. Droplets can be categorized into small droplets (initial size ≤30 μm or ≤10 μm as droplet nuclei), medium droplets (30-80 μm) and large droplets (>100 μm) according to the exposure characteristics. Droplets up to 100 μm, particular the small ones, can contribute to both short-range and long-range airborne routes. For the face-to-face talking scenario, the intake fraction and deposition fractions of droplets on the face and facial mucosa of the susceptible were up to 4.96%, 2.14%, and 0.12%, respectively, indicating inhalation is the dominant route. The exposure risk from a talking infector decreases monotonically with the interpersonal distance, while that of nasal-breathing generated droplets maintains a relatively stable level within 1.0 m. Keeping an angle of 15° or above with the expiratory flow is efficient to reduce intake fractions to <0.37% for small droplets. Adjusting the orientation from face-to-face to face-to-back can reduce exposure to small droplets by approximately 88.0% during talking and 66.2% during breathing. A higher ventilation rate can reduce the risk of exposure to small droplets but may increase the risk of transmission via medium droplets by enhancing their evaporation rate. This study would serve as a fundamental research for epidemiologist, healthcare workers and the public in the purpose of infection control.

（266 words）

Keywords: Respiratory droplets, close contact, airborne route, interpersonal distance, relative position, COVID-19

1. Introduction

As of August 2022, more than 617 million cases of infection and more than 6 million deaths have been attributed to COVID-19 worldwide (WHO, 2022). Respiratory activities, such as breathing, talking, and coughing, produce droplets, which range from submicron to millimeters in diameter; these droplets are the main carriers of SARS-CoV-2 and other respiratory viruses (Johnson et al., 2011; CDC, 2021; Leung, 2021). Respiratory droplets are a complex combination of components like water, proteins, and nonvolatile ionic solutes and may contain pathogens at times (Effros et al., 2002). These droplets, once expired into indoor environments, immediately lose water through evaporation and finally reach equilibrium; at this stage, they are referred to as droplet nuclei and range from 25% to 33.33% of their initial size (Duguid, 1946; Liu et al., 2017). Droplets sized 10 μm evaporate in 0.066–1.52 s, whereas those sized 100 μm evaporate in 6.63–199.0 s (Wei and Li, 2015). Respiratory droplets are transported in two stages, with the primary being the expiratory flow, followed by secondary dispersion via room airflow (Wei and Li, 2016). The droplet size is the main factor that determines the droplet dispersion and deposition characteristics (Morawska, 2006). Small droplets or droplet nuclei <5 μm in diameter remain suspended in indoor environments for long periods, increasing the risk of long-distance spread (WHO, 2006); in contrast, large droplets may travel for ≤2 m and deposit readily due to the gravitational force (Xie et al., 2007; Wei and Li, 2015).

Respiratory viruses can be transmitted through the large-droplet spray route, short- or long-range airborne routes, and fomites (Wei and Li, 2015; Leung, 2021; Wang et al., 2021). The spray route was first proposed by Flügge (1897) and was positively acknowledged by Chapin (1910). Large droplets can be easily visualized using high-speed cameras (Bourouiba et al., 2014). Maintaining a safe distance and frequently sanitizing ones hands were considered the main precautionary measures against COVID-19 at the beginning of the pandemic; high-grade personal protective equipment (e.g., N95 masks) was only used in aerosol generating procedures (WHO, 2020; Greenhalgh et al., 2021). However, fine droplets have been shown to be important carriers of influenza viruses (Linsley et al., 2010; Milton et al., 2013) and, recently, of SARS-CoV-2 (Coleman et al., 2021). In light of the increasing evidence of COVID-19 transmission via the airborne route, for example, the outbreak among members of a choir (Hamner et al. 2020) and the animal transmission study (Sia et al., 2020), the US Centers for Disease Control and Prevention recognized airborne transmission as a route for COVID-19 transmission in July 2021 (CDC, 2021), more than 1.5 years into the pandemic. Studies have also highlighted the importance of efficient ventilation designs, air filtration, and properly fitting face masks in the prevention of COVID-19 (Tang et al., 2021).

The relative importance of the large droplet and airborne routes as well as the cutoff size to differentiate aerosols (the major cause of infection via the airborne route) from droplets remain under debate (Gao et al., 2021; Wang et al., 2021). To clarify these issues, quantification of the risk of exposure to different-sized droplets is essential; these issues are also affected by factors such as the type of respiratory activity, human contact behavior, and ventilation. Cough-expired droplets have drawn the most attention in the literature, followed by breathing-expired droplets (Chao et al., 2009). In real situations, however, face-to-face coughing rarely occur, and presymptomatic and asymptomatic transmissions of COVID-19 are notable concerns (Arons et al., 2020; Johansson et al., 2021). Thus, the role of talking in the transmission of COVID-19 was recently identified as follows: the high-speed laryngeal jet formed during vocalization readily breaks up the mucus to produce droplets (Asadi et al., 2018; Coleman et al., 2021). Besides, the

face-to-face exposure scenario has been extensively studied (Liu et al., 2007); in contrast, not many studies have addressed human contact behavior in indoor environments, which is a complicated concept. Compared with maintaining proper social distancing, being face-to-back with the infector may be more effective in reducing the risk of infection (Liu et al., 2022). Moreover, ventilation reduces the risk of airborne transmission, and researchers usually adopt well-mixing assumptions in evaluating this risk. However, ventilation also impacts the expiratory flow during close contact (Li, 2021b). The evaporation and deposition of respiratory droplets complicate the exposure characteristics, especially when the droplets are approximately 50 μm in diameter (Wei and Li, 2015). In the present study, we systematically examined the effects of occupant behavior and ventilation on exposure to different-sized respiratory droplets. It would provide novel insight into the transmission mechanism of respiratory infections like COVID-19, and facilitate the quantification of transmission risk and the development of effective control measures against COVID-19 in indoor environments.

2. Methods

2.1 Mechanically ventilated three-dimensional room model.

A generic quadruple room with ceiling-supply and floor-level-exhaust ventilation (Figure 1) was built to systematically investigate the release of respiratory droplets from the infector individual (red) and the risk of exposure for susceptible individuals (grey) via direct inhalation or deposition of droplets on the facial membrane.

The room dimensions were 7.0 (L) × 5.3 (W) × 2.7 (H) m^3. The areas of the two air inlets and four air outlets were 0.23 m^2 and 0.15 m^2, respectively. The four persons were all 1.7 m in height. The susceptible persons maintained an interpersonal distance of 0.3–2.5 m with the infector. Susceptible 1 (S1) faced the infector in multiple orientations (denoted as α) and relative positions (denoted as β, Figure 1b).

<Fig. 1>

2.2 Numerical methods.

An unstructured tetrahedral grid was created using ICEM CFD 19.0 (ANSYS, USA) to discretize the volume of the mechanically ventilated 3-dimensional room model. The total number of cells used in the final mesh was determined using a grid-independence test. Meshes comprising 6.1, 10.5, and 13.7 million elements were compared. A grid resolution of 10.5 million was found to be sufficient for predicting the velocity magnitude and droplet dispersion characteristics (Figure 2a, 2b). The grid was rendered denser near walls including human body surfaces (about 10 mm) than the free stream domain (up to 50 mm). Three prism layers were created near walls, with the first layer height being 1.5 mm to guarantee y^+ values below 1. The final mesh with closeups on the manikin and wall is shown in Figure 2c.

<Fig. 2>

The velocity field of the room is obtained by solving the conservation equations of mass, energy, and momentum on ANSYS Fluent 18.0 (ANSYS, USA). The shear stress transport (SST) k–ω model was adopted. Boussinesq's hypothesis was applied to account for the buoyancy force. The

semi-implicit method for pressure-linked equations (SIMPLE) algorithm was used to model pressure-velocity coupling in airflows. Second-order discretization schemes were used for the convection and viscous terms of the governing equations.

Next, respiratory droplets are released by the infector via talking or via nasal breathing. Because the volume fraction of the droplets in this study was small, a discrete phase model based on the Lagrangian method was adopted to calculate the trajectories of the droplets. This method considers droplets to be a discontinuous discrete phase affected by drag, gravitational, and additional forces. Pressure and virtual mass forces, which are very small in magnitude due to the large density ratio of droplets to air, were thus usually ignored (Zhao et al., 2004). Moreover, the discrete random walk model was used to account for the effects of turbulence on droplet dispersion (Wang et al., 2012). At least 42,880 droplets of each size were released and tracked to ensure statistical accuracy after a droplet number independence test. Treating the droplets as water droplets during evaporation provides adequate accuracy, and the evaporation process is terminated if the droplet reaches the size of droplet nuclei, which is approximately 1/3 of its initial size under RH$\leqslant$67%, as has been proven in our previous study (Liu et al., 2017).

2.3 Model validation.

Two experimental benchmarking studies were referred to validate the turbulence and discrete phase models. First, a full-scale environmental chamber (4.91 × 2.44 × 4.31 m^3) with an under-floor air distribution system and four heated human simulators standing in the room was validated. The model and boundary conditions were the same as those used by Zhang and Chen (2006). A comparison of the simulated and measured velocities and temperature is presented in Figure 2e, which shows a reasonable agreement. Furthermore, the turbulence model adopted in our study could accurately model the jet flow (Figure S1, Supplementary Materials).
For the second validation, the geometric model and boundary conditions were set as the same conditions used by Lai and Chen (2006). The model dimensions were 0.8 (L)× 0.4 (W)× 0.4 (H) m^3, with the inlet and outlet both being 0.04 × 0.04 m^2. The inlet velocity was 0.225 m/s, and the outlet was set as a pressure outlet, with the other walls set with no-slip wall boundary conditions. As shown in Figure 2d, particle deposition fraction was accurately predicted using the numerical method adopted in our study. Actually, the SST k–ω model with enhanced wall treatment that guarantees a y^+ of $\leq$1 predicts the turbulence kinetic energy k more accurately in the laminar sublayer compared with the k-ε model as has been proved in our previous studies (Guo, et al, 2020; Wan et al., 2021). It is equivalent to the near wall correction method proposed by Matida et al., (2004).

2.4 Boundary conditions.

The boundary conditions are summarized in Table 1. Ventilation requirements vary among occupancy categories; for example, the ventilation requirement is 5.1 L/(s·person) for restaurant dining rooms, 6.7 L/(s·person) for lecture classrooms, 9.4 L/(s·person) for aircraft cabins, 23.0 L/(s·person) for gyms, 50 L/(s·person) for hospital general wards, et al. (ASHRAE, 2019; WHO, 2009). In this study, we set the ventilation rate to 4.2–66.7 L/(s·person) or 15-240 m^3/(h·person) to investigate the effects of ventilation rates on droplet exposure. The air supply velocity corresponding to the current room geometry was set to 0.036–0.288 m/s, and the air change rate was 0.61-9.76 air changes per hour (ACH). The temperature of the supply air in all conditions was 17°C, and the relative humidity was 52%.

<Table 1>

Non-slip boundary conditions were applied to all walls in the CFD simulations, and all walls were assumed to be adiabatic. The basic metabolic heat generated by an adult is approximately 70 W/m^2 and is mainly dissipated from the body through convection and radiation. In this study, we considered only heat dissipation via convection, which accounts for approximately 50% of the total heat generated by the human body; accordingly, we set the heat flux density to 35 W/m^2 (Topp et al., 2002). The infector can release respiratory droplets either by talking or via nasal breathing, which is a complex process. To simplify the process, we considered the respiratory activities as exhalation at a constant speed. The source patient's expiratory area was 1.8 cm^2, and the exhalation speed was 5 m/s for talking and 30 L/min for nasal breathing (Gupta et al., 2010). The temperature of the expiratory flow was 35°C, and the relative humidity was 100% (Hoppe, 1981).

The airflow–particle interaction was considered a one-way coupling, and the effects of the droplets on the airflow field were ignored. Particle–particle interactions was also ignored. The aerodynamic diameters of the investigated particles were 1–100 μm for talking and 3 μm for nasal breathing. The density of each particle was 1,000 kg/m^3. The initial velocity of the particles was equal to that of the expiratory airflow. The boundary effects of the droplets at the walls and exhaust outlets were set as "trap" and "escape," respectively, indicating that the trajectory calculations terminated at the walls and exhaust outlets, respectively.

3. Results

The infector may release respiratory droplets of various sizes while talking or nasal breathing, and a susceptible individual may be subject to exposure and thus infection because of inhaling the droplets or by droplet deposition on their face (and facial mucosa). To evaluate the risk of exposure, *intake fraction* was defined as the ratio of droplets inhaled by a susceptible to the total droplets exhaled by the infector, and *deposition fraction* as accounts for the droplet deposition onto the face or facial mucosa of a susceptible individual.

3.1 Exposure during the face-to-face talking scenario

Face-to-face talking imposes the highest risk on susceptible individuals. The flow field, dispersion patterns of respiratory droplets with various initial diameters, and intake/deposition fractions of susceptible individuals are shown in Figure 3. An uprising thermal plume formed around the human body owing to differences in the temperature between the skin and ambient air. The thermal plume starts from the floor level by drawing ambient air and grows thicker and accelerates as it rises. The maximum velocity at the breathing level and above the occupant's head was >0.2 m/s, consistent with that in previous studies (Murakami, 2004). The thermal plume usually acts as a protective air curtain for susceptible individuals; however, when in proximity with the infector, this curtain can be easily penetrated by the respiratory jet (Figure 3a). Next, the respiratory jet was brought upward such that it interacted with the uprising thermal plume and readily reached the room ceiling (Figure 3b). Both the velocity and concentration of the fine droplets (surrogated by water vapor) decreased with the jet traveling distance and, as a result of the complex mouth geometry, the decay rates were much higher than those of the ideal round jet having an equivalent opening (1.5 cm) and velocity (5 m/s) (Figure 3c). The respiratory

flow readily mixed with the room air, and the centerline velocity dropped from 5 m/s to 1 m/s within 0.2 m, whereas the distance required by an ideal round jet is approximately 0.5 m (Wei and Li, 2015). In this study, the jet half-angle was approximately 14.0° for an expiratory jet emitted from a realistic mouth, while it is only 9.1° for an ideal turbulent round jet.
The evaporation time for small droplets, which can closely follow the airflow, was negligible (Figure 3d). The intake fractions of a susceptible individual and the deposition fractions of droplets on the susceptible individual's face under various distances from the infector are shown in Figure 3g. The intake fraction and deposition fractions on the face and facial mucosa for small droplets (≤30 μm) at a distance of 0.5 m were 4.96%, 2.14%, and 0.12%, respectively; the inhalation route was found to impose the highest risk of infection. These fractions almost decreased monotonically with a larger interpersonal distance and dropped to 0.75%, 0.02%, and 0%, respectively, at a distance of 2.5 m. For medium-sized droplets, the evaporation time was longer (Figure 3e), ranging from seconds to tens of seconds depending on the relative humidity (Wei and Li, 2015); moreover, neither their intake fraction nor deposition fraction were larger than those of the small droplets, which contradicts the assumptions from the conventional understanding of the spray route (WHO, 2020). In addition, the intake fraction of medium droplets peaked at 1.5 m as droplet nuclei are more easily inhaled after evaporation. In contrast, large droplets (≥100 μm) get deposited readily after release (Figure 3f), and their maximum travel distance before complete settlement out of the jet was only approximately 0.5 m in this study, which was much shorter than the 1.0 m predicted under the ideal round jet assumption (Xie et al., 2007). Although some droplet nuclei could be lifted upward again by room air, the intake fractions of the 100 μm droplets were <0.05% for all distances. Larger droplets (e.g., those of size 150 μm) did not impose an exposure risk at all in the investigated scenarios. In our study, the facial mucosa (including the eyes and lips, 11.4 cm^2 in area) accounted for only 5.5% of the total face area. At an interpersonal distance of 1.0 m, droplets of size < 100 μm deposited uniformly on the whole face. The deposition ratio of the facial mucosa to the whole face decreased when larger interpersonal distances were maintained, because this action led to the upward tilting of the expiratory flow and no droplets depositing on the lips. Detailed deposition data are provided in Table S1 and Table S2 of the Supplementary Materials.

<Fig. 3>

3.2 Effect of face orientation and relative position on droplet exposure

In real situations, susceptible individuals may adopt various face orientations (α) or relative positions (β, Figure 1b) when talking to the infector; the risks of exposure for susceptible individuals were systematically evaluated under each of these scenarios (Figure 4). Avoiding directly facing the infector is helpful in reducing exposure to small droplets, but such an orientation may make the intake fractions of medium droplets fluctuate. The respiratory jet of the infector moved upward more readily when interacting with the thermal plume, and the concentration of the small droplets in the susceptible individual's breathing zone decreased relative to that in the face-to-face talking scenario (Figure 4a). The intake fractions of the 5 μm droplets were 3.32% at $\alpha = 0°$, 0.74% at $\alpha = 90°$, and 0.40% at $\alpha = 180°$(Figure 4b). However, medium droplets, for example those of diameter 80 μm, settled out of the expiratory jet due to the gravitational force, evaporated on their way settling to the floor, and were re-entrained by the susceptible's thermal plume and brought upward to his breathing zone, as shown in Figure 4a. The most droplets are re-entrained if the susceptible stands laterally to the infector, resulting into a peak intake fraction value of 80 μm droplets as revealed in Figure 4b.

<Fig. 4>

A more efficient maneuver for reducing the risk of exposure was to face away from the respiratory flow by adjusting one's relative position with the infector (β). The respiratory flow, which is high in droplet concentration in the early stages, reached the room ceiling after approximately15 s and then went through further rapid dilution after it was disrupted by the ventilation flow (Figure 4c). This flow was diluted by approximately 30 times when traveling a distance of 1.0 m and by approximately 300 and 700 times when reaching the susceptible individual at $\beta = 15°$ (Susceptible 1) and 90° (Susceptible 2), respectively (Figure 4d). At an angle of 15° and for 5 μm droplets, the intake fraction decreased to 0.37%; a similarly decrease from 1.69% to 0.08% was observed for 50 μm droplets at a relatively larger angle of 30°, owing to the re-entrainment mechanism of the thermal plume, as mentioned above (Figure 4e).

Moreover, the deposition of droplets on the susceptible individual's face was obvious only in the face-to-face talking scenario (Figure 4f). At a low intake fraction in which $\beta \geq 15°$, the droplet deposition on the face was almost negligible, and no droplet deposition was noted on the facial mucosa.

3.3 Exposure to the nasal-breathing infector

Unlike talking, nasal breathing emits only small droplets (<3 μm, Johnson et al., 2011), and the expiratory flow travels downward from the nostril (Figure 5a). The vertical momentum of the expiratory flow is gradually counteracted by buoyancy forces, and the flow rises after it reaches the lowest point (Figure 5b). In this study, the horizontal and vertical displacements of the breathing flow at its lowest point were 0.43 m (L_{f1}) and 0.91 m (H_f), respectively. Thus, the risk of exposure of the susceptible individual to the infector is relatively insensitive to the interpersonal distance when the susceptible individual directly faces the infector in close proximity. The intake fraction ranged from 1.17% to 1.51% for interpersonal distances of <1.0 m; it peaked at 0.7 m (Figure 5c) and suddenly dropped to 0.39% at 1.5 m. It is worth to mention that a closer distance doesn't necessarily lead to a higher exposure risk, because the breathing flow is more diluted after impacting on the infector's body and rising with the thermal plume. In particular, the maximum distance the droplets traveled before the expiratory flow mixed with the ventilation air without any obstruction by the susceptible individual was 1.34 m (L_{f2}). Because breath-exhaled droplets are small and the respiratory flow does not directly impact the susceptible individual's face, the deposition fraction was relatively low, i.e., <0.12% under face-to-face breathing conditions.

<Fig. 5>

Avoiding face-to-face interactions by changing the face orientation α or relative position β helps reduce the risk of exposure (Figure 5d). The face-to-back position ($\alpha = 180°$) is most frequently used in public places such as subways and airplanes; in this position, the expiratory flow is blocked by the human body and thermal plume, resulting in an intake fraction of only 0.51% at an interpersonal distance of 0.7 m. Adopting appropriate susceptible-infector relative positions may be even more efficient in avoiding infection. Owing to the abovementioned directional characteristics of the expiratory flow, the intake fraction was only 0.23% when $\beta = 45°$.

3.4 Effect of ventilation rate on droplet exposure

It has been well recognized that the dispersion of respiratory droplets is dominated by the respiratory jet in the initial stage and by room airflow in the later stage after the jet diminishes. However, this study shows the ventilation rate also affects the expiratory flow by diluting or deflecting it, as shown in Figure 6a. A jet entrains background air as it travels, grows in dimension, and then decays in velocity and concentration of matters it carries. Thus, a higher ventilation rate implies a lower background concentration, which dilutes the respiratory jet more efficiently. For example, the centerline water vapor density of the expiratory jet at 0.7 m is reduced from 10.6 g/m^3 to 10.2 g/m^3 (by 3.8%) if the ventilation rate is increased from 30 m^3/(h·person) to 90 m^3/(h·person). Microenvironment of Infector and S1 is complex under the combined effect of respiratory jet, ventilation airflow and the thermal plume (Figure 6b); generally, water vapor densities of the bulk air surrounding the respiratory jets are approximately 8.1 g/m^3 and 7.7 g/m^3, respectively, under the two different ventilation rates.

<Fig. 6>

Small droplets (e.g., those 5 μm in diameter) behave like water vapor; their intake fraction decreased from 3.32% to 2.84% (i.e., by 14.5%) when the ventilation rate was increased from 30 m^3/(h·person) to 90 m^3/(h·person) (Figure 6e). However, larger droplets (30 and 50 μm in diameter) behaved in the opposite manner (increased by 1.7% and 54.4%, respectively) until strong ventilation deflected the expiratory flow at 120 m^3/(h·person). As mentioned above, the water vapor density inside/surrounding the respiratory jet only drops by about 4%, but the 50 μm droplets are quite sensitive to that small change of humidity. That is probably because their terminal setting velocity lies between 8.3 mm/s (16.7 μm, droplet nuclei) and 74.0 mm/s (50 μm, initial size), which is comparable with the jet entrainment velocity that ranges from 17.1 mm/s (x= 1.0 m) to 86.6 mm/s (x= 0.1 m); the jet entrainment coefficient is set as 0.057 (Wei and Li, 2015). A portion of these droplets fall out of the jet (Figure 6c), but decrease of the gravitational settling velocity resulting from a faster evaporation rate would help them reman inside (Figure 6d). Once relatively large droplets settled out of the jet, they tend to deposit and are difficult to be inhaled by the susceptible. On the other hand, a higher rate of ventilation readily dilutes the droplets; the intake fraction of 80 μm droplets peaks under 60 m^3/(h·person) as affected by the two above-mentioned mechanism.

The risk of long-distance airborne exposure is much smaller than that of short-distance airborne exposure. The intake fractions of the 5 μm droplets were 2.84%-3.47% and 0.11%-0.17% under the short- and long-distance airborne routes, respectively, at an interpersonal distance of 1.0 m; the corresponding values were 1.49%-2.61% and 0.03%-0.04% for the 50 μm droplets. Generally, a higher ventilation rate results in a lower long-distance airborne exposure risk when the droplet size is small (Figure 6f). However, this reduction was smaller compared with that of the well-mixing theory; the former was reduced by only 36.1% when the ventilation rate was increased from 15 to 90 m^3/(h·person), while the latter was reduced by 83.3% under similar conditions. This can be attributed to the airflow pattern in the investigated scenario, as revealed in Figure 3; droplet deposition is significant, especially at the ceiling. On the other hand, the intake fraction of relatively large droplets (≥50 μm) increases with the ventilation rate because a faster evaporation process prolongs their suspension in air (Figure 6d), until the ventilation rate is increased to 240 m^3/(h·person) when the dilution effect dominates.

4.Discussions

The airborne and droplet-borne transmission of respiratory infectious disease transmission traditionally differ by a 5 μm or 10 μm cutoff size of the droplets involved (WHO, 2016), and the popular concept of the large-droplet spray route was first proposed by Flügge (1897) and Chapin (1910). Wells (1934) first proposed the concept of 'large droplets'; that is, droplets >100 μm will settle on the ground before they completely evaporate. However, our recent study has revealed that a susceptible individual may inhale both large and small droplets during close contact with a talking or coughing infector, and this 'inhalation route' poses a much higher risk of infection than the 'direct spray route' (Chen et al., 2020; Li, 2021a). Findings in this study are more robust as the CFD technique applied herein clarify the inhalation flow and thermal plume in high resolution, and adopted realistic mouth geometry. It is shown that droplets >100 μm travel a limited distance (less than 0.5 m), owing to the complex geometry of the mouth; in contrast, an ideal round jet the travels approximately 1.0 m (Xie et al., 2007).

It is clearly revealed in this study that droplets with an initial diameter of ≤100 μm can also contribute to the long-distance airborne route, and small droplet nuclei (<10 μm) are more prone to be efficiently transmitted via the airborne route owing to their prolonged suspension times. To the best of our knowledge, our systematic study is the first to comprehensively examine these cutoff sizes. Figure 7 summarizes the intake fractions as a function of the droplet's initial diameters under various interpersonal distances under our investigated scenarios. For small droplets (<30 μm initial diameter or 10 μm droplet nuclei diameter), the intake fraction is not sensitive to the droplet size. It decreases drastically if the droplet size further increases, and drops to zero for 100 μm droplets. The terminal setting velocity of the 10 μm droplet nuclei was only 3 mm/s in still air, and it took >10 min for these nuclei to deposit on the floor (Wei and Li, 2015). It is worth mentioning that only the inhalable droplets, defined as those ≤10 μm in diameter, can reach lower respiratory tract after inhalation (ICRP, 1994).

<Fig. 7>

Droplet nuclei <10 μm accounted for 99.83% of the total talking-generated droplets in number but contributed only 0.02% in volume (Morawska et al., 2009; Johnson et al., 2011). However, small droplet nuclei < 5 μm have been proved as important carriers of influenza virus and SARS-CoV-2 (Linsley et al., 2010; Milton et al., 2013; Coleman et al., 2021); medium or large droplets are difficult to sample using available instruments, NIOSH bioaerosol sampler for example, with an upper sampling limit of 10 μm. An alternative method based on CFD simulations indicated that medium and large droplets mainly originate from the oral cavity and that viral content is much lower in the mouth than in the pharynx, larynx, and the lower respiratory tract (Guo et al., 2020). Moreover, pathogens initiate an infection by depositing onto the facial mucosa or being inhaled and then depositing in the respiratory tract. Inhaled droplets >10 μm in diameter deposit in the upper respiratory tract (including the oral cavity, pharynx, and larynx), and only droplets ≤ 2.5 μm in diameter reach the alveolar region (ICRP, 1994). However, dose–response data at different locations of the respiratory tract are lacking (Gao et al., 2021).

Maintaining an interpersonal distance is widely recommended as one of the major actions against the spread of COVID-19. Distancing is efficient if the infector is performing nasal breathing (Figure 5) but may be compromised if the expiratory flow is horizontal and strong (Figure 3G). The findings of our study may have overestimated the horizontal penetration distance of the

expiratory flow given the steady-jet implications; thus, additional studies assessing transient respiratory activities are needed. A more efficient method to protect susceptible individuals from droplet exposure is to adjust their relative position with the infector by taking advantage of the directional characteristics of the expiratory flow (Figure 4). Moreover, the face orientation of the susceptible individual is also an important parameter, especially in situations such as waiting on a subway platform (Wei et al., 2022; Liu et al., 2022).

In our study, both short-range and long-range airborne routes were affected by the ventilation rate. At an interpersonal distance of 1.0 m, intake fractions of 5 μm droplets via the short- and long-distance airborne routes decreased by 18.2% and 36.1%, respectively, when the ventilation rate increased from 15 to 90 $m^3/(h \cdot person)$. These reduction could be as high as 33.11% and 83.3% according to the entrainment theory of an ideal round jet and the well-mixing assumption of the room (Wei and Li, 2015; Li, 2021b). However, on the other hand, a higher ventilation rate may increase the transmission risk contributed by relatively large droplets because of the decrease in water vapor density and increase in droplet evaporation rate in our investigated scenario. The intake fractions of 50 μm droplets via both the short- and long-distance routes increased by 75.2% and 48.1%, respectively, under the aforementioned change in the ventilation rate. It is worth mentioning that, although medium droplets (30-80 μm) are almost negligible in number compared with small droplets (≤30 μm), their volume is about 15 times that of small ones (Johnson et al., 2011). This phenomenon contradicts the traditional understanding that a higher ventilation rate is beneficial for reducing the transmission risk of respiratory infections. It has been proved in our previous study that medium droplets, rather than small droplets or large droplets, are sensitivity to humidity from the perspective of dispersion pattern (Wei and Li, 2015); it is expected from the results of Figure 6 that a higher humidity probably results into a sharp increase of the droplets' gravitational deposition rate and decrease of the sequential exposure risk. As relative humidity and temperature of the supply air were kept constant throughout this study, this phenomenon requires a further and more thorough investigation for making appropriate ventilation strategies.

The coefficient of the droplet deposition rate in a ventilated room is usually 0.1–5.5 for 1–5 μm particles, and a larger droplet size or greater background ventilation increases the deposition rate (Thatcher et al., 2002). In contrast, in our study, the droplet deposition rate coefficient was 18.6–34.0 for 5 μm droplets. Due to the buoyancy effects of the horizontal expiratory flow and the thermal plume, the droplets accumulate at the ceiling level, and 21.5%–32.7% of these droplets deposit on the ceiling, accounting for approximately 50% of the total deposition. The deposition rate coefficient was only 7.8% for the 3 μm droplets expired via nasal breathing because these droplets were well mixed with the room air before reaching the ceiling. Our results indicate that although floor-level exhausts are popular in ventilation design, ceiling-level exhausts may help eliminate respiratory droplets efficiently. Our results are consistent with those of a previous study that compared different ventilation patterns and concluded that fine particles were removed more efficiently by ceiling-level exhausts than by floor-level exhausts and that large particles were mainly removed by deposition rather than ventilation (Qian et al., 2010).

Although simplified scenarios were investigated in this study were, they provide fundamental insights for understanding the risk of exposure to different-sized droplets. Our study also has some limitations. Occupant movement and the transient properties of expiratory activities would complicate the dispersion and exposure of respiratory droplets. In this study, the transient nature of respiratory air flow and head/body movement were ignored, which is a major limitation.

Secondly, room layout and its furniture are not considered, which will, in particular, affect the long-range airborne route. Thirdly, more parameters defining close contact behaviors can be introduced in the future, for example, the height difference in breathing zones of the infector and the susceptible. Fourthly, respiratory droplets were treated as water droplets, and the relative humidity and temperate of supply air were kept constant throughout the study. Relative humidity, in particular, affects the evaporation and dispersion characteristics of respiratory droplets; hydroscopicity of protein content carried by droplets affect the evaporation process more significantly at humid conditions (Liu et al., 2017), which needs further investigations. In addition, we evaluated the exposure probability of respiratory droplets by assessing the intake and deposition fractions, which are not equivalent to exposure risk (Dai and Zhao, 2022). Additional studies evaluating the risk of exposure by considering the viral content in different-sized droplets and the dose–response coefficient after exposure are essential.

5. Conclusions

In this study, the exposure to respiratory droplets of various sizes via inhalation or by deposition on the face (and facial mucosa) were systematically investigated when a susceptible individual shared a room with an infector who was talking or nasally breathing. The exposure characteristics were highly related to the type of respiratory activity and droplet diameter. Moreover, influencing factors such as interpersonal distance, face orientation, relative position to the infector, and ventilation rate were quantitatively investigated. The short-range airborne route, or inhalation route, exposes much higher exposure risks comparing with the direct spray route and the long-range airborne route. Appropriate position to the infector and face orientation are as efficient as keeping social distance. As for ventilation rate, a higher value is beneficial to reduce both the short-range and long-range exposure risk from small droplets, but may lead to more inhalation of medium droplets (30-100 μm) due to their prompted evaporation rate. Further investigations in virus contents of different-sized droplets, droplet exposure characteristics in realistic indoor environments and dose-response coefficients after droplet exposure are necessary for better quantification of transmission risks of respiratory infections.

Acknowledgement

The authors thank Prof. Bin Zhao, Tsinghua University, for providing insightful suggestions during this study. This study was financially supported by the National Natural Science Foundation of China (52178092 & 52108067), the Natural Science Foundation of Zhejiang Province (LY20E080018), and the Basic Research Funds for the Central Government 'Innovative Team of Zhejiang University' under contract number (2022FZZX01-09).

Data availability

All data generated and analysed during this study are included in the Article and its Supplementary Materials. Fluent case and data files will be provided upon request to Dr. Jianjian Wei (weijzju@zju.edu.cn) and Dr. Nan Zhang (zhangn@bjut.edu.cn).

References

Atkinson J, Chartier Y, Pessoa-Silva CL, Jensen P, Li Y, Seto WH, editors. Natural Ventilation for Infection Control in Health-Care Settings. Geneva: World Health Organization; 2009

Arons MM, Hatfield KM, Reddy SC, et al. Presymptomatic SARS-CoV-2 infections and transmission in a skilled nursing facility. *N. Engl. J. Med.*, 2020, 382:2081-2090
Asadi S, Wexler AS, Cappa CD, et al. Aerosol emission and superemission during human speech increase with voice loudness. *Sci. Rep*., 2019, 9:1-10
ASHRAE. ANSI/ASHRAE Standard 62.1-2019, Ventilation for Acceptable Indoor Air Quality. American Society of Heating, Refrigerating, and Air-Conditioning Engineers, Inc., 2019, Atlanta, USA
Bourouiba L, Dehandschoewercker E, Bush JWM. Violent expiratory events: on coughing and sneezing. *J. Fluid Mech*., 2014, 745:537-563
Centers for Disease Control and Prevention. Scientific brief: SARS-CoV-2 Transmission_Updated May 7, 2021. https://www.cdc.gov/coronavirus/2019-ncov/science/science-briefs/sars-cov-2-transmission.html#anchor_1619805240227/
Chao CYH, Wan MP, Morawska L, et al. Characterization of expiration air jets and droplet size distributions immediately at the mouth opening. *J. Aerosol Sci*., 2009, 40:122-133
Chapin CV. The sources and modes of infection. Wiley, 1910
Chen W, Zhang N, Wei J, et al., Short-range airborne route dominates exposure of respiratory infection during close contact. *Build. Environ.*, 2020, 176:106859
Coleman KK, Tay DJ, Tan KS, et al. Viral load of SARS-CoV-2 in respiratory aerosols emitted by COVID-19 patients while breathing, talking, and singing. *Clin. Infect. Dis.*, 2022, 74:1722-1728
Dai H, Zhao B. Association between the infection probability of COVID-19 and ventilation rates: An update for SARS-CoV-2 variants. *Build. Simul.*,2022. https://doi.org/10.1007/s12273-022-0952-6
Duguid JF. The size and duration of air-carriage of respiratory droplets and droplet-nuclei. *J. Hyg.*, 1946, 4: 471-480
Effros RM, Wahlen K, Bosbous M, et al. Dilution of respiratory solutes in exhaled condensates. *Am. J. Resp. Crit. Care. Med.*, 2002, 165:663-669
Flügge C. Uber Luftinfection. *Z Hyg Infektionskr*. 1897, 25:179-224
Gao CX, Li Y, Wei J, et al. Multi-route respiratory infection: when a transmission route may dominate. *Sci. Total Environ.*, 2021, 752:141856
Greenhalgh T, Jimenez JL, Prather KA, et al. Ten scientific reasons in support of airborne transmission of SARS-CoV-2. *Lancet*, 2021, 397:1603-1605
Guo Y, Wei J, Ou C, Liu L, Sadrizadeh S, Jin T, Tang L, Zhang Y, Li Y. Deposition of droplets from the trachea or bronchus in the respiratory tract during exhalation: A steady-state numerical investigation, *Aerosol Sci Tech*, 2020, 54(8): 869-879
Gupta JK, Lin CH, Chen Q. Characterizing exhaled airflow from breathing and talking, *Indoor Air*, 2010, 20:31-39
Hamner L, Dubbel P, Capron I, et al. High SARS-CoV-2 attack rate following exposure at a choir practice. *Morb. Mortal. Wkly. Rep.*, 2020, 69:606-610
Hoppe P. Temperature of expired air under varying climatic conditions. *Int. J. Biometeorol.*, 1981, 25:127-132
International Commission on Radiological Protection (ICRP). Human respiratory tract model for radiological protection. ICRP publication 66. Ann. 1994, 24:1-3
Johansson MA, Quandelacy TM, Kada S. et al. SARS-CoV-2 transmission from people without COVID-19 symptoms. *JAMA Netw. Open*, 2021, 4:e2035057
Johnson GR, Morawska L, Ristovski ZD, et al. Modality of human expired aerosol size distributions. *J. Aerosol Sci*., 2011, 42:839-851

Lai ACK and Chen F. Modeling particle deposition and distribution in a chamber with a two-equation Reynolds-averaged Navier-Stokes model. *J. Aerosol Sci.*, 2006, 37:1770-1780
Li Y. Basic routes of transmission of respiratory pathogens—A new proposal for transmission categorization based on respiratory spray, inhalation, and touch. *Indoor Air*, 2021a, 31(1):3-6
Li Y. Hypothesis: SARS-CoV-2 transmission is predominated by the short- range airborne route and exacerbated by poor ventilation. *Indoor Air*, 2021b, 31:921-925
Lindsley WG, Blachere FM, Thewlis RE, et al. Measurements of airborne influenza virus in aerosol particles from human coughs. *PLoS One*, 2010, 5:1-6
Liu L, Li Y, Nielsen PV, Wei J, Jensen RL. Short-range airborne transmission of expiratory droplets between two people. *Indoor Air*, 2017, 27:452-462
Liu L, Wei J, Li Y, et al. Evaporation and dispersion of respiratory droplets from coughing. *Indoor Air*, 2017, 27:179-190
Liu X, Dou Z, Wang L, et al. Close contact behavior-based COVID-19 transmission and interventions in a subway system. *J. Hazard. Mater*, 2022, 129233
Matida EA, Finlay WH, Lange CF, Grgic B. Improved numerical simulation of aerosol deposition in an idealized mouth-throat. *J Aerosol Sci*, 2004, 35:1-19
Milton DK, Fabian MP, Cowling BJ, et. al. Influenza virus aerosols in human exhaled breath: particle size, culturability, and effect of surgical masks. *PLOS Pathog.*, 2013, 9:1-7
Morawska L. Droplet fate in indoor environments, or can we prevent the spread of infection? *Indoor Air*, 2006, 16:335-347
Morawska L, Johnson GR, Ristovski ZD, et al. Size distribution and sites of origin of droplets expelled from the human respiratory tract during expiratory activities. *J Aerosol Science*, 2009, 40(3): 256-269
Murakami S. Analysis and design of micro-climate around the human body with respiration by CFD. *Indoor Air*, 2004, 14:144-56
Qian H and Li Y. Removal of exhaled particles by ventilation and deposition in a multibed airborne infection isolation room. *Indoor Air*, 2010, 20:284-297
Sia SF, Yan LM, Chin AWH, et al. Pathogenesis and transmission of SARS-CoV-2 in golden hamsters. *Nature*, 2020, 583:834-838
Tang S, Mao Y, Jones RM. Aerosol transmission of SARS-CoV-2? evidence, prevention and control. *Environ. Int.*, 2020, 144:106039
Thatcher TL, Lai ACK, Moreno-Jackson R, et al. Effects of room furnishings and air speed on particle deposition rates indoors. *Atmos. Environ.*, 2002, 36:1811-1819.
Topp C, Nielsen PV, Sorensen D. Application of computer simulated persons in indoor environmental modeling. *Build. Eng.*, 2002, 108:1084-1089
Wan J, Wei J, Lin Y, Zhang T. Numerical investigation of bioaerosol transport in a compact lavatory, *Buildings*, 2021, 11(526)
Wang M, Lin CH, Chen Q. Advanced turbulence models for predicting particle transport in enclosed environments. *Build. Environ.*, 2012, 47:40-49
Wei J and Li Y. Airborne spread of infectious agents in the indoor environment. *Am. J. Infect. Control*., 2016, 44:102-108
Wei J and Li Y. Enhanced spread of expiratory droplets by turbulence in a cough jet. *Build. Environ.*, 2015, 93:86-96
Wei J, Zhu S, He F, et al. Numerical investigation of airborne transmission of respiratory infections on the subway platform. *GeoSci. Front.*, 2022, 101384
Wells WF. On air-borne infection study II. Droplets and droplet nuclei. *Am. J. Epidemiol.*, 1934, 20:611-618

World Health Organization. Infection prevention and control of epidemic-and pandemic prone acute respiratory infections in healthcare-WHO guidelines, 2014
World Health Organization. Transmission of SARS-CoV-2 : implications for infection prevention precautions, 2020. https://www.who.int/news-room/commentaries/detail/transmission-of-sars-cov-2-implications-for-infection-prevention-precautions/
World Health Organization. Weekly Operational Update on COVID-19, 2022. https://www.who.int/emergencies/diseases/novel-coronavirus-2019/situation-reports/
Xie X, Li Y, Chwang ATY. et al. How far droplets can move in indoor environments. *Indoor Air*, 2007, 17:211-225
Zhang Z and Chen Q. Experimental measurements and numerical simulations of particle transport and distribution in ventilated rooms. *Atmos. Environ.*, 2006, 40:3396-3408
Zhao B, Zhang Y, Li X, Yang X, Huang D. Comparison of indoor aerosol particle concentration and deposition in different ventilated rooms by numerical method. *Build. Environ.*, 2004, 39:1-8

Supplementary Materials

Effects of occupant behavior and ventilation on exposure to respiratory droplets in indoor environments by Jianjian Wei, Lei Wang, Tao Jin, Yuguo Li, Nan Zhang

Table S1. Intake fractions during face-to-face interactions with a talking infector. The ventilation rate is 30 m^3/h/person.

Initial droplet diameter (μm)	Intake fraction (%)			
	0.5 m	1.0 m	1.5 m	2.5 m
1	4.96	3.30	1.43	0.56
5	5.05	3.32	1.41	0.49
10	4.75	3.25	1.51	0.60
20	4.41	3.22	1.55	0.74
30	3.061	3.20	1.66	0.81
50	0.94	1.69	1.91	0.91
80	0.22	0.21	0.06	0.03
100	0.03	0.03	0.05	0.01
150	0	0	0	0

Table S2. Deposition fractions during face-to-face interactions with a talking infector. The ventilation rate is 30 m^3/h/person.

Initial droplet diameter (μm)	Deposition fraction on the face (%)				Deposition fraction on facial mucosa (%)			
	0.5 m	1.0 m	1.5 m	2.5 m	0.5 m	1.0 m	1.5 m	2.5 m
1	2.15	1.10	0.25	0.02	0.12	0.07	0.005	0
5	2.12	1.06	0.27	0.02	0.09	0.07	0.002	0
10	2.00	1.03	0.29	0.02	0.12	0.05	0.02	0

20	1.87	1.13	0.28	0.02	0.11	0.06	0.02	0
30	1.90	1.17	0.37	0.01	0.11	0.08	0.01	0
50	1.75	0.72	0.46	0.03	0.15	0.03	0.002	0
80	0.20	0.12	0.01	0.002	0.01	0.002	0	0
100	0.04	0.01	0.01	0	0	0	0	0
150	0	0	0	0	0	0	0	0

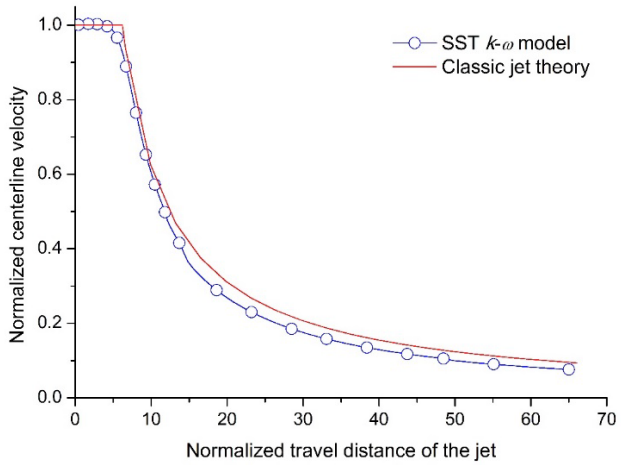

Figure S1. Normalized centerline velocity of an ideal round jet predicted using the SST k–ω model against classic jet theory

Figure 1. Illustration of the investigation scenarios.
(a)Three-dimensional model of the investigated mechanically ventilated room. Fresh air is supplied from the ceiling, and the exhaust is located at the floor level. The infector (red) can talk or perform nasal breathing. (b) α, face orientation of a susceptible individual; β, relative position of a susceptible individual to the infector.

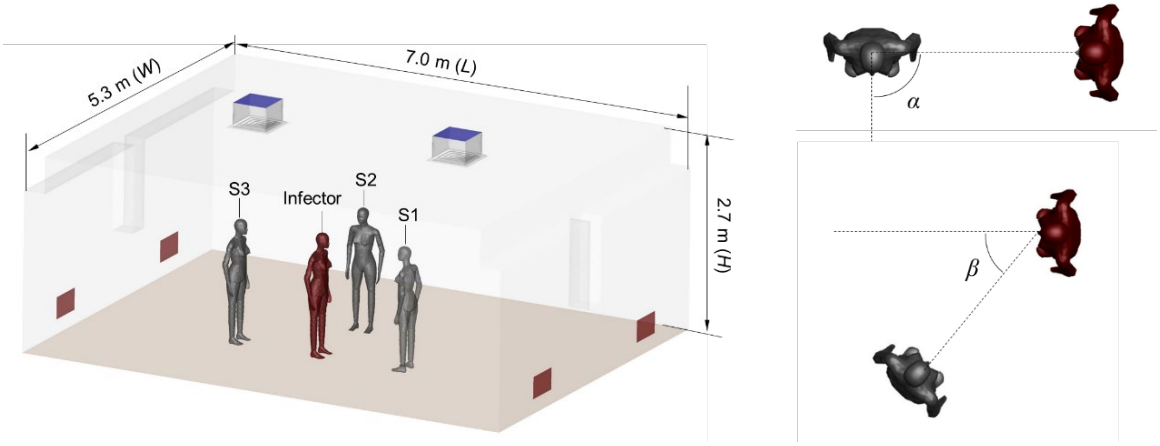

(a) (b)

Figure 2. Robustness of the numerical methods
(a) Grid independence test of velocity magnitude over the infector's head. (b) Grid independence test of the intake fractions of 5-μm-sized droplets. (c) Illustration of the final mesh. (d, e) Validation of the numerical methods against experimental benchmarking studies about the velocity and temperature field by Zhang and Chen (2006) and particle deposition rate by Lai and Chen (2006). V1-V7 represent seven different measurement locations for the airflow.

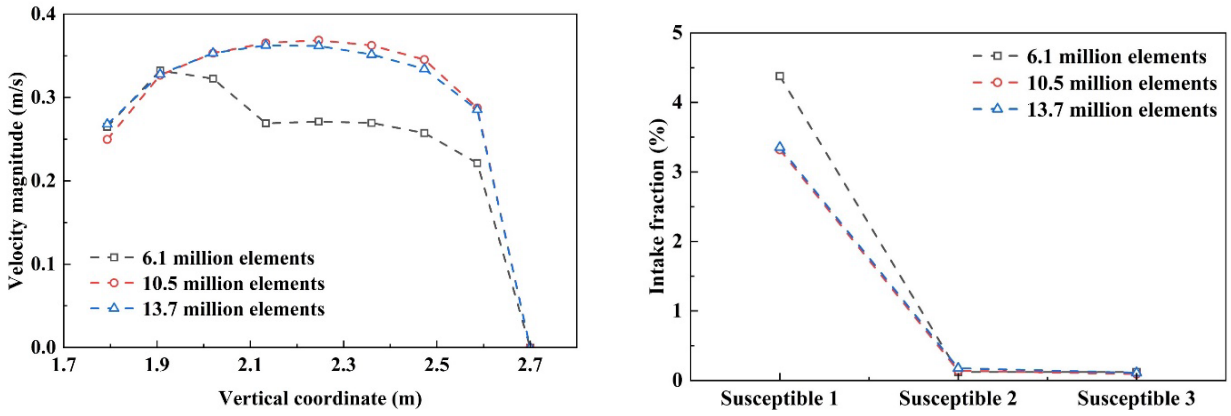

(a) (b)

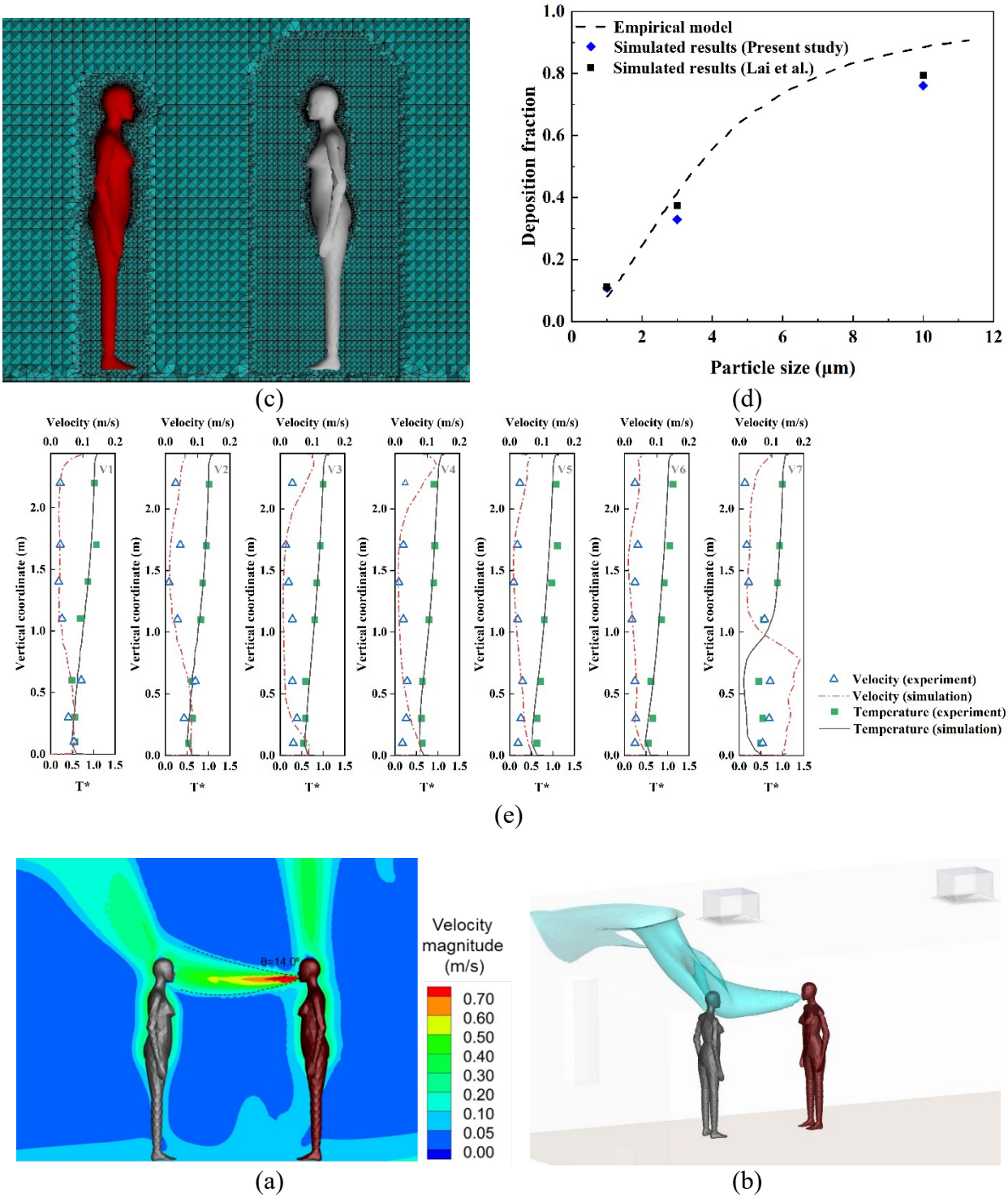

Figure 3. Characterization of the flow field and risk of exposure during face-to-face talking. (a) Velocity field indicating the interaction between the respiratory jet and thermal plumes. (b) Isosurface of the water vapor density at $\bar{\rho} = 0.017$. (c) Decay of the centerline velocity and water vapor density as functions of jet traveling distance. (d-f) The dispersion pattern of droplets with initial diameters of 5, 50, and 100 μm, respectively. The distance between the infector and susceptible in (a-f) is 1.0 m, and outdoor air is supplied from the ceiling at a ventilation rate of 30 m^3/h/person. (g) Intake fraction and deposition fraction of the susceptible as a function of

droplet diameter and exposure distance under the same ventilation rate. The facial mucosa accounts for 5.5% of the total face area.

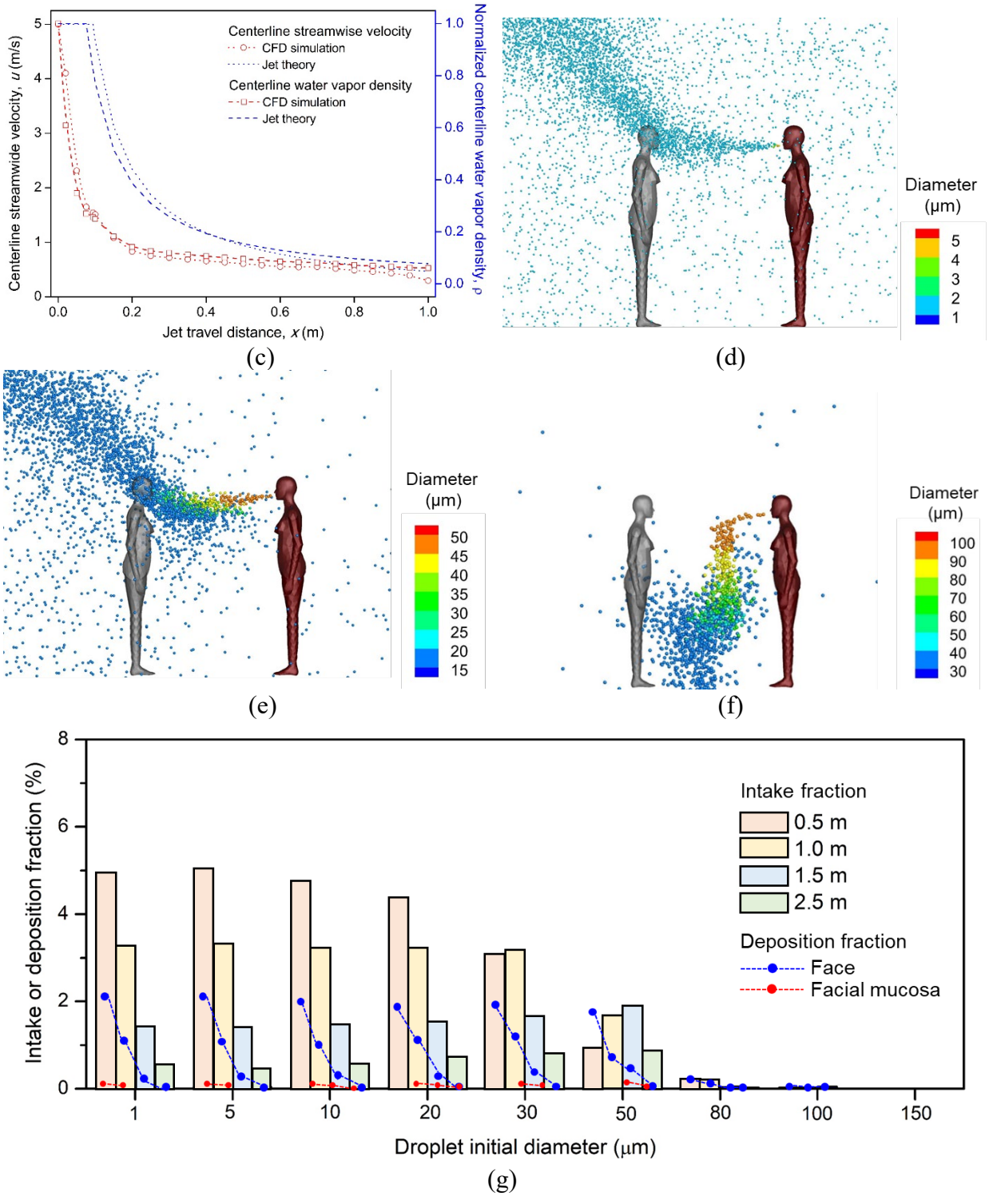

Figure 4. Risk of exposure for the susceptible individual based on their face orientation and angle relative to a talking infector at an interpersonal distance of 1.0 m.
(a) Dispersion pattern of 5 μm and 80 μm (initial diameter) droplets at $\alpha = 90°$. (b) Intake fractions under different face orientations, α. (c) Age of the 5 μm droplets and (d) isosurfaces of

water vapor density at $\beta = 15°$, showing the directional characteristics of the respiratory flow and fine droplets. (e) Intake fractions of the susceptible individual under various angles with respect to the respiratory jet, β. (f) Ratio of the deposition fraction (on the face) to the intake fraction under various scenarios. Outdoor air was supplied from the ceiling at 30 $m^3/(h \cdot person)$.

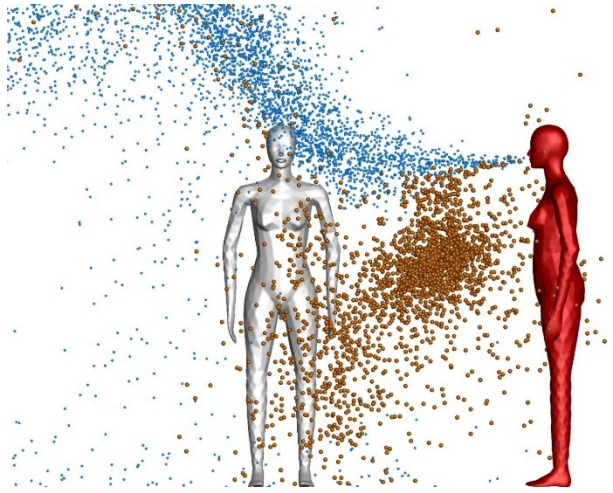

(a)

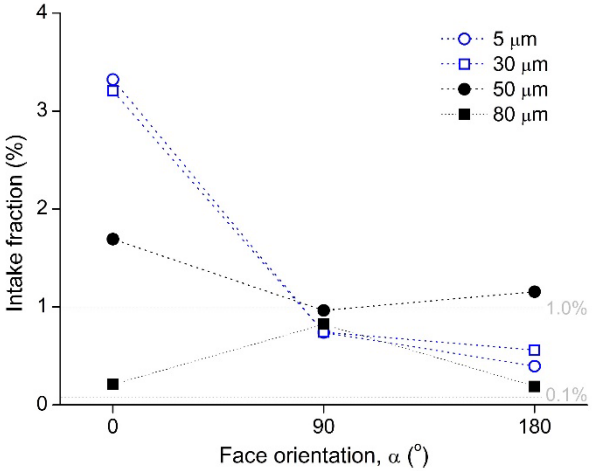

(b)

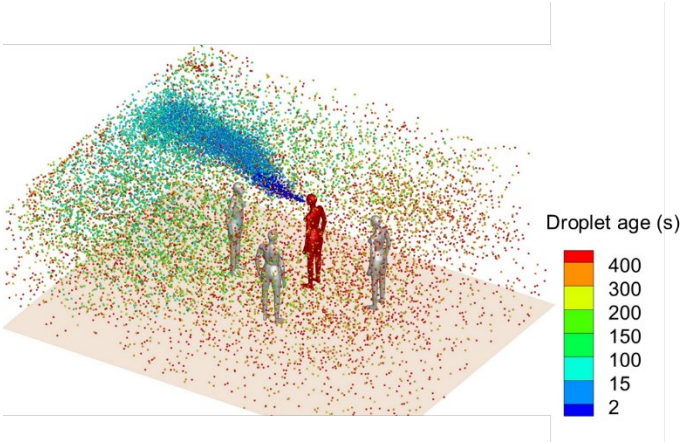

(c)

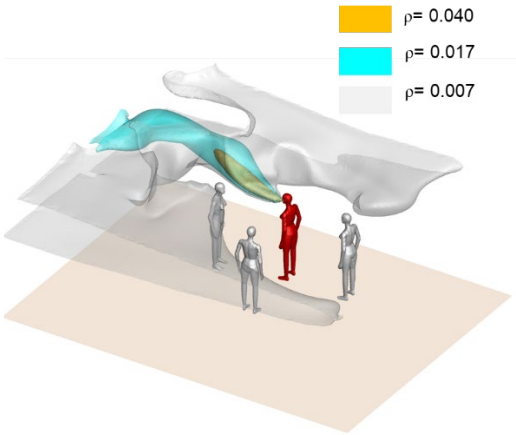

(d)

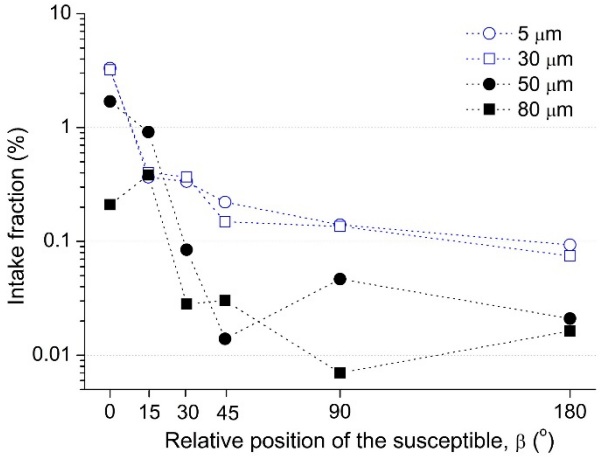

(e)

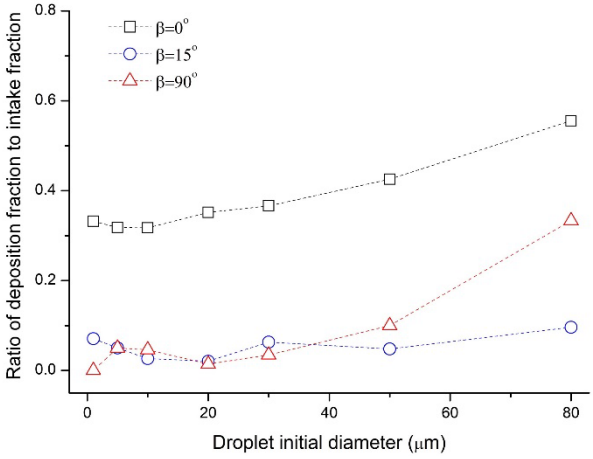

(f)

Figure 5. Flow field and risk of exposure when the infector is nasal breathing at 30 L/min. Outdoor air was supplied from the ceiling at 30 m^3/h/person.
(a) Velocity field. (b) Isosurfaces of water vapor density. The interpersonal distance was 1.0 m. (c) Intake and deposition fractions of 3 μm droplets at various distances. (d) Intake fractions of 3 μm droplets with various face orientations α and angles with respiratory jet β.

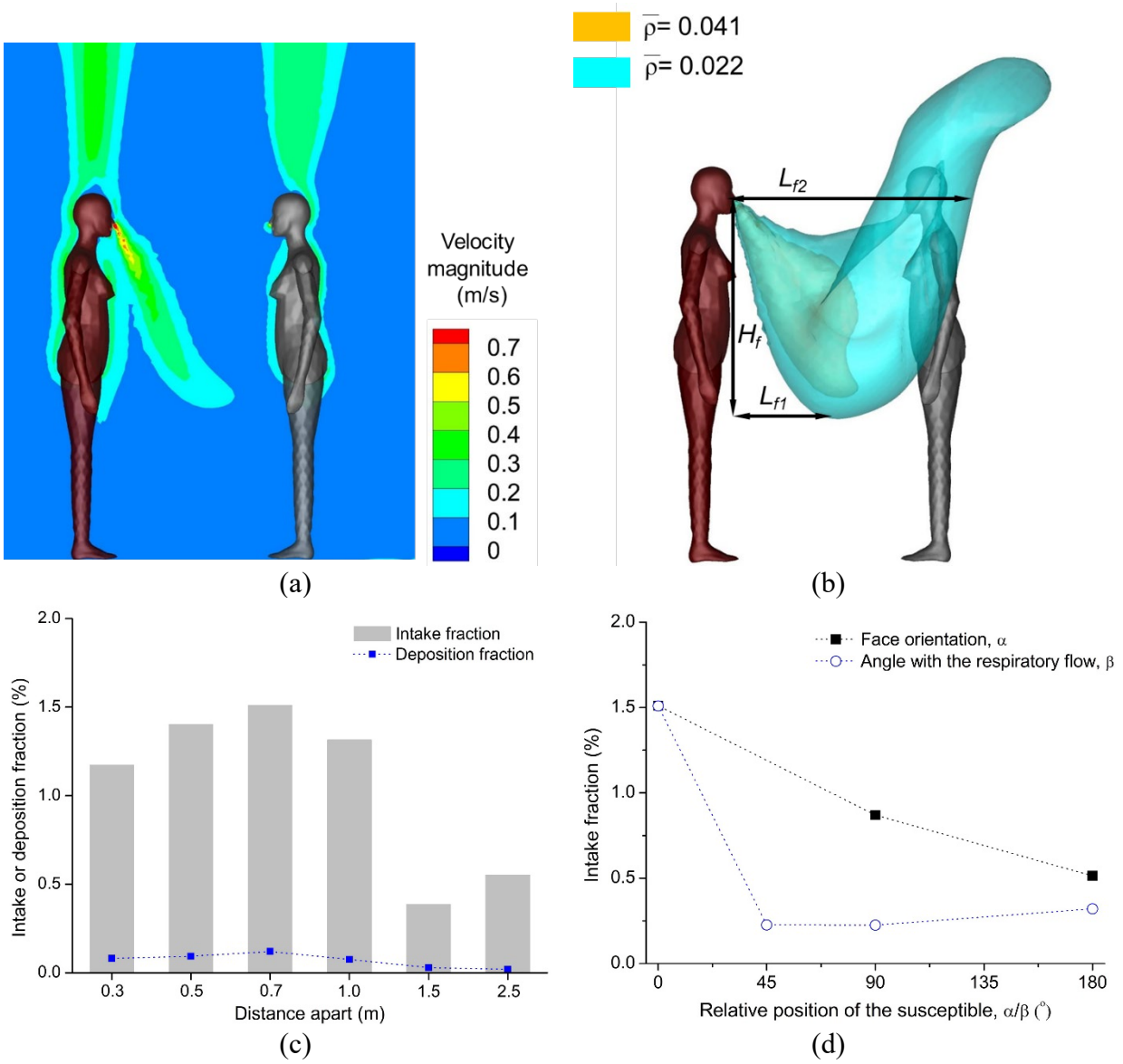

Figure 6. Effect of ventilation rate on expiratory flow and intake fractions. Distance between the infector and susceptible was 1.0 m.
(a) Iso-surface of water vapor density at 9.2 g/m^3. (b) Water vapor density in the microenvironment. (c), (d) Droplet age under 30 m^3/(h·person) and 90 m^3/(h·person), respectively. Only droplets with age ≤40s are shown. (e) Intake fractions of S1, corresponding to short-range airborne route. (f) Average intake fractions of S2 and S3, representing the long-range airborne exposure risk, under different ventilation rates.

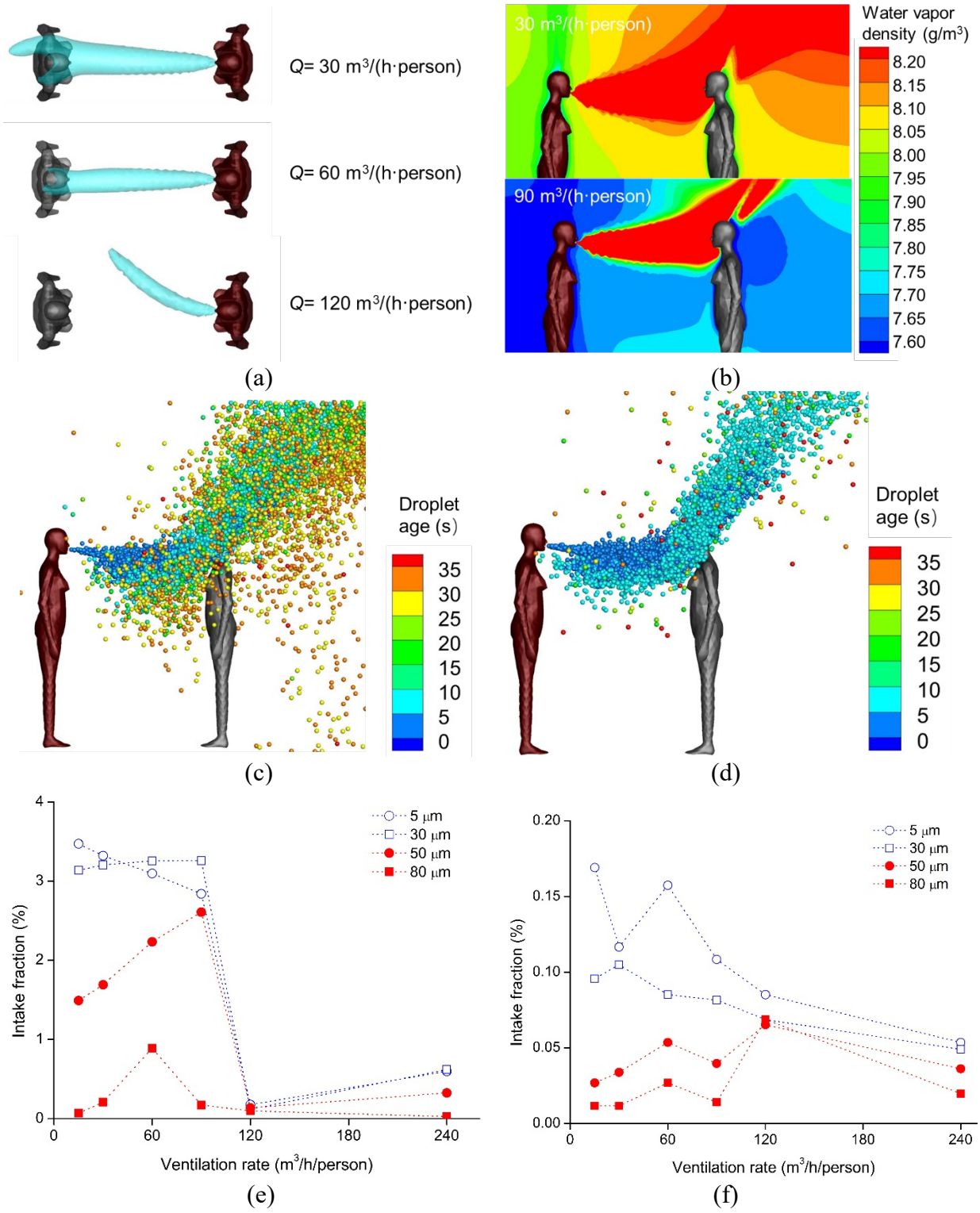

Figure 7. Intake fractions for the face-to-face talking scenario (S1) and the long-range airborne route (average values for S2 and S3). Zero-value data points are not shown.

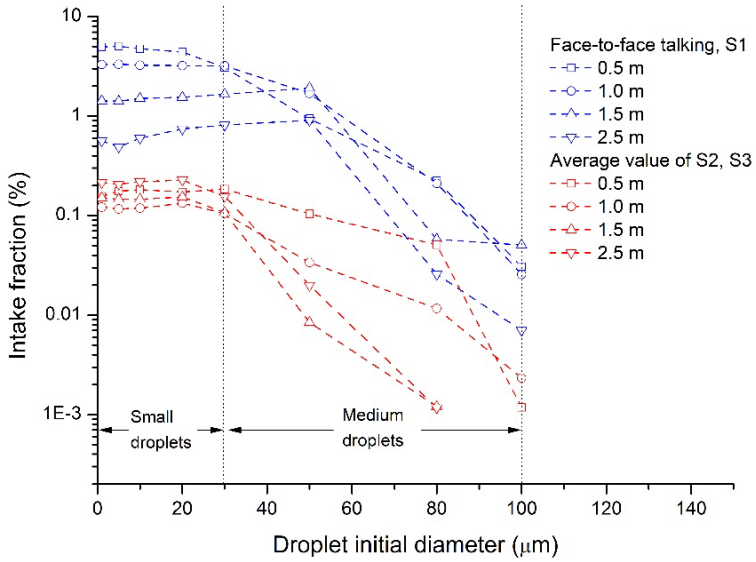
Intake fraction (%)
10
1
0.1
0.01
1E-3
0
20
40
60
80
100
120
140
Droplet initial diameter (μm)
Small droplets
Medium droplets
Face-to-face talking, S1
0.5 m
1.0 m
1.5 m
2.5 m
Average value of S2, S3
0.5 m
1.0 m
1.5 m
2.5 m

Table 1. A summary of the boundary conditions

Boundary name	**Boundary type**	**Boundary setup**
Air supplies	Velocity inlet	15-240 $m^3/(h \cdot person)$ (0.036-0.576 m/s or 0.61-9.76 ACH); 17°C (temperature), 52% (relative humidity)
Air exhausts	Pressure outlet	'Escape' for droplets
Infector's mouth or nostrils	Velocity inlet	5 m/s for talking and 30 L/min for nasal breathing; 35°C (temperature), 100% (relative humidity)
Initial diameter of the respiratory droplets	N/A	1–100 μm for talking and 3 μm for nasal breathing
Susceptible person's nostrils	Velocity outlet	'Escape' for droplets
Room wall	Wall	Adiabatic; 'trap' for droplets
Skin	Wall	35 W/m^2; 'trap' for droplets
Face orientation, α	N/A	0°, 90°, 180° denoting face-to-face, face-to-side, and face-to-back scenarios, respectively
Relative position, β	N/A	0°–180°